ELSEVIER

Journal of Nuclear Materials 249 (1997) 39–45

journal of nuclear materials

The influence of alloying elements on the hot-dip aluminizing process and on the subsequent high-temperature oxidation

H. Glasbrenner *, E. Nold, Z. Voss

Forschungszentrum Karlsruhe, Institut für Materialforschung III, PO Box 3640, D-76021 Karlsruhe, Germany

Received 24 February 1997; accepted 4 June 1997

Abstract

For hot dip aluminizing (HDA) an Al melt was doped with one of the elements Mo, W or Nb with a nominal composition of about 1 wt%. In case of W, the nominal composition was achieved, not so for Mo and Nb. The influence of these elements on the coating formed and on the following oxidation process was investigated. Hot dip aluminizing was carried out at 800°C for 5 min under dry Ar atmosphere. The oxidation experiments were performed at 950°C for 24 h in air. Compared to the HDA processes with pure Al, the addition of the alloying elements lead to thinner intermetallic layers. A change in the oxidation behavior was observed as well concerning the suppression of internal oxidation and the formation of dense and close oxide scales. © 1997 Elsevier Science B.V.

1. Introduction

In the water-cooled blanket concept, the liquid alloy Pb–17Li serves as breeder material. During the process, the alloy is pumped with extreme low velocity. Therefore, the tritium partial pressure is significant in Pb–17Li in which the tritium solubility is low. To reduce the diffusion of tritium through the structural material into the cooling water circuit a tritium permeation barrier on the steel is necessary for economic and safety reasons. A martensitic steel DIN 1.4914 (Martenisitic for NET, MANET) is foreseen as structural material.

The permeation rate can be reduced sufficiently with an alumina or iron aluminide coating on MANET [1–5]. The coating process must be compatible with the heat-treatment of the steel to produce a δ-ferrite free martensitic phase; therefore the bulk mechanical properties are not affected. The most promising process is to coat a complex geometry of steel from the inside or the outside by hot dip aluminizing (HDA). The components to be coated could be immersed into an Al melt or the liquid melt could be pumped through the components. As a result of Al diffusion into the steel an intermetallic layer is formed on the surface.

First experiments to coat MANET by using a melt of pure Al were quite successful, however, the following high-temperature oxidation process showed some uncertainties [6,7]. The oxide scale formed is not uniform and dense, and a broad band of pores in between the intermetallic layer can be observed due to the different diffusion rates of Fe and Al (Kirkendall effect). The inward diffusion of Al into the steel matrix is much faster than the outward diffusion of Fe out of the matrix. In particular, the defects could seriously impair the effectiveness of the coating as a permeation barrier.

It is a known fact that alloying elements can have a significant influence on the oxidation reaction and the diffusion behavior of different elements in a compound [8–10]. A beneficial effect on the oxidation reaction has been reported for Nb, Mo and W [11]. By using the hot dip aluminizing process, iron aluminides with a low content of the elements mentioned above were prepared. In this paper, their influence on the oxidation behavior of iron aluminides containing Nb, Mo and W will be discussed.

2. Experimental

MANET specimens consisted of plates of 60×15 mm^2 and 1.5 mm in thickness. The material is taken from the

* Corresponding author. Tel.: +49-7247 823 723; fax: +49-7247 823 956; e-mail: glasbrenner@imf.fzk.de.

PII S0022-3115(97)00186-4

Table 1
The amounts of Al and the respective alloying element which were melted together

Aluminum	Alloying element	Nominal composition
100.459 g	W: 1.00 g	1.015 wt%
92.09 g	Nb: 0.87 g	0.930 wt%
91.17 g	Mo: 0.92 g	0.921 wt%

NET-heat (No. 50806) produced by Saarstahl Völklingen, Germany, with the following composition (in wt%): C 0.10, Si 0.18, Mn 0.76, P 0.004, S 0.005, Cr 10.37, Ni 0.65, Mo 0.58, V 0.21, Nb 0.16, B 0.0075, N 0.032, Al 0.007, Co 0.005, Cu 0.01, As 0.01, Sb 0.0002, Sn 0.001, Zr 0.008 and Fe balance. A thick scale on the surface consisting mainly of Cr_2O_3 was removed by sandblasting. Afterwards, the cleaned sheets were heat treated under vacuum in three steps in order to condition the steel: at 965°C for 2 h, 1075°C for 30 min and at least at 750°C for 2 h.

The 0.5 mm thick Al sheets used had a purity of 99.5%. The elements added to the Al melt, existed in the following form: W was used as band, Nb was added as foil with 125 μm in thickness and Mo existed as 0.5 mm thick sheet. The nominal composition of the prepared Al–X (X = W, Mo, Nb) alloys is listed in Table 1.

The liquid temperatures are around 700°C for the systems Al–X (X = W, Mo, Nb) with X = 1 wt% [12–14]. Hence, the solubility of W, Mo and Nb in Al at 800°C is quite low. The melts were produced by using the same operation process for all systems. Firstly, aluminum was heated in a sintered crucible made of Al_2O_3 placed in a muffle furnace under dry Ar atmosphere in a glove-box up to 800°C. Secondly, the alloying element is given in small pieces into the Al melt. The melt was stirred time by time for 1 h. This was followed by the hot dip aluminizing (HDA) process. A sample of the melt was taken for analysis just before and directly after the HDA process. The results of the analysis are given in Table 2.

The nominal composition of the Al–W melt with 1 wt% W was achieved after 1 h. After the HDA process, the content of W has decreased. In case of the other two metals, Mo and Nb, the nominal composition was not reached. The higher contents of Mo and Nb after the HDA process show, that the dissolution of the metals was not finished after 1 h when the HDA process started. During the next 30 min of the HDA process the dissolution of the metals in the Al melt could be continued and therefore, the concentration is higher after the HDA process. The content of the other analyzed metals in the melts, components of the steel, is higher after the HDA process because a slight dissolution of the steel components into the melt has occurred during the heating and aluminizing procedure of the steel sheets in the melt. The maximum change is detected for the main components Fe and Cr of the steel. The range of increase of these two elements in the three different melts is in the same order of magnitude.

For the HDA process, cold MANET sheets were dipped in the melt at 800°C for 5 min. During this procedure the specimen to be coated was moved in the melt time by time. This is necessary for a complete covering, otherwise some uncovered regions would remain on the steel surface. All together, five specimens were immersed one after another in each Al–X melt. For comparison, MANET steel sheets were hot dipped in pure, unalloyed Al melt under the same conditions. The following high temperature (HT) oxidation was performed in air at 950°C for 30 h in a conventional furnace followed by a heat treatment at 750°C for 2 h to condition the steel. Furthermore, the oxidation process was investigated in a thermobalance.

Specimens were analyzed after the HDA process and after the HT oxidation on the surface with energy dispersive X-ray analysis (EDX). Polished cross-sections of the specimens were applied by X-ray microanalysis (XMA), by Auger electron spectroscopy (AES) and metallographic methods. Additionally, Vickers micro hardness measurements were carried out on the different intermediate layers on the steel before and after the HT oxidation in regions

Table 2
The composition of the different melts before and after the HDA process (in wt%)

	Al–W melt		Al–Mo melt		Al–Nb melt	
	before HDA	after HDA	before HDA	after HDA	before HDA	after HDA
W	1.01	0.84				
Mo			0.17	0.28		
Nb					0.044	0.056
Fe	0.64	3.62	0.34	3.34	0.72	3.33
Cr	0.094	0.41	0.013	0.35	0.062	0.36
Cu	0.0015	0.0016	0.0011	0.0026	0.0014	0.0015
Mg	0.0057	0.0058	0.0028	0.0030	0.0041	0.0060
Mn	0.014	0.036	0.0045	0.028	0.0088	0.032
Ni	0.050	0.070	0.013	0.039	0.027	0.040
Ti	0.021	0.019	0.020	0.021	0.019	0.020
Zn	< 0.005	< 0.005	< 0.005	< 0.005	< 0.005	< 0.005

without pores and cracks. The load was 0.05 N, reached after 15 s.

3. Results

3.1. HDA specimens

After the HDA process, an aluminide layer can be recognized on each steel surface independent of the Al melt used (Fig. 1). The connection between this layer and the steel seems to be good although the transition is rather frayed out. Micro cracks in all aluminide layers were present perpendicular to the surface. It is well-known that the major aluminide phase formed by the HDA process is the brittle η-Al_5Fe_2-phase [15,16]. The maximum and minimum thickness of the aluminide layers formed in the different melts is shown in Table 3. The aluminide layer formed in the Al–Mo melt seems to be the most uniformed one, the variation in thickness is small. In case of the aluminide layer out of the Al–Nb melt, the irregularity of the aluminide layers increases. The thinnest part of an aluminide layer was found on the specimens which were dipped in the Al–W melt. The average values of the measured micro hardness of the three different layers are with 843 $HV_{0.05}$ (Al–W), 880 $HV_{0.05}$ (Al–Nb) and 886 $HV_{0.05}$ (Al–Mo) all in the same range. This corresponds to a micro hardness value of 835 $HV_{0.02}$ given in the literature [16] for the brittle intermetallic compound Al_5Fe_2.

Fig. 1. Cross-sectional views of aluminized MANET steel sheets which were hot dipped in a melt of (a) Al–W, (b) Al–Nb or (c) Al–Mo. The large crystals located near the brittle η-Al_5Fe_2-phase are marked with arrows.

Table 3
The thickness of the aluminide layer on the MANET steel formed at 800°C during 5 min immersion time

Thickness of the aluminide layer	Al–W melt	Al–Nb melt	Al–Mo Al–melt	Al melt
In minimum	6 μm	12 μm	16 μm	50 μm
In maximum	38 μm	40 μm	44 μm	100 μm

The surface of each specimen was analyzed with EDX. The elements detected are Al as main component, and small amounts of Fe and Mg. In no case, the alloying elements W, Nb or Mo could be found. The concentration of these elements seems to be under the detection limit for this method (0.1–0.2 wt%).

The cross-sections of the specimens were analyzed by AES. For all Al–X specimens (X = W, Mo, Nb) the aluminide layer exists solely of an Fe–Al phase with a low content of Cr, no X element could be detected in this region. The top layer exists mainly of pure Al in which some Fe_xAl_y crystals are embedded. In addition, in all Al–X specimens other crystals located near the aluminide layer can be observed (see also Fig. 1a–c). These large crystals consist of Fe–Cr–W–Al (Fig. 2a) and Fe–Cr–Mo–Al (Fig. 2b), resp., with Al as the main component. Nb could not be detected in the Al–Nb specimens although in these specimens other shaped crystals could be observed as well. Probably the concentration of Nb is under the limit of detectability of AES, which varies between 0.1 and 1 at.%.

3.2. HDA specimens after oxidation process

In the cross-sectional view, two different layers on the steel can be observed on the etched HDA (Al–X) specimens at 950°C for 30 h in air: a top layer and a so-called intermediate layer, which are separated by a porous band. The thickness of this band is about 45 μm for the alloying

elements W and Nb, and around 30 μm for Mo (Fig. 3). In case of Mo, the pores are larger than for the HDA specimens alloyed with W and Nb. The intermediate layer consists of radial crystals, which were formed by diffusion during high temperature oxidation. The transition from the intermediate layer to the steel side is clearly defined. Neither cracks nor pores can be detected in the these layers.

The scale morphology of the oxides investigated with scanning electron microscopy (SEM) showed completely different surfaces on each specimen. The only conformity is the roughness which could be found on each surface.

Analysis by EDX showed Al to be the main component in the oxides scale. Using a 30 keV electron beam, the atomic ratio Al:Fe is about 9:1. Cr was found to be around 1.3 at.%. Nb and Mo, resp., could not be detected in the surface, but the alloying element W was identified with 0.7 at.% in average by this method. The penetration depth is larger than the thickness of the scale. Therefore, not only the oxide scales were analyzed but also a small part of the diffusion top layer.

Additionally, the 1–2 μm thick oxide scales of the specimens were examined by XMA. In all cases, a qualitative overview spectrum was measured. The result is identical for all Al–X specimens. The spectra showed only Al, O and a low content of the steel components Fe and Cr.

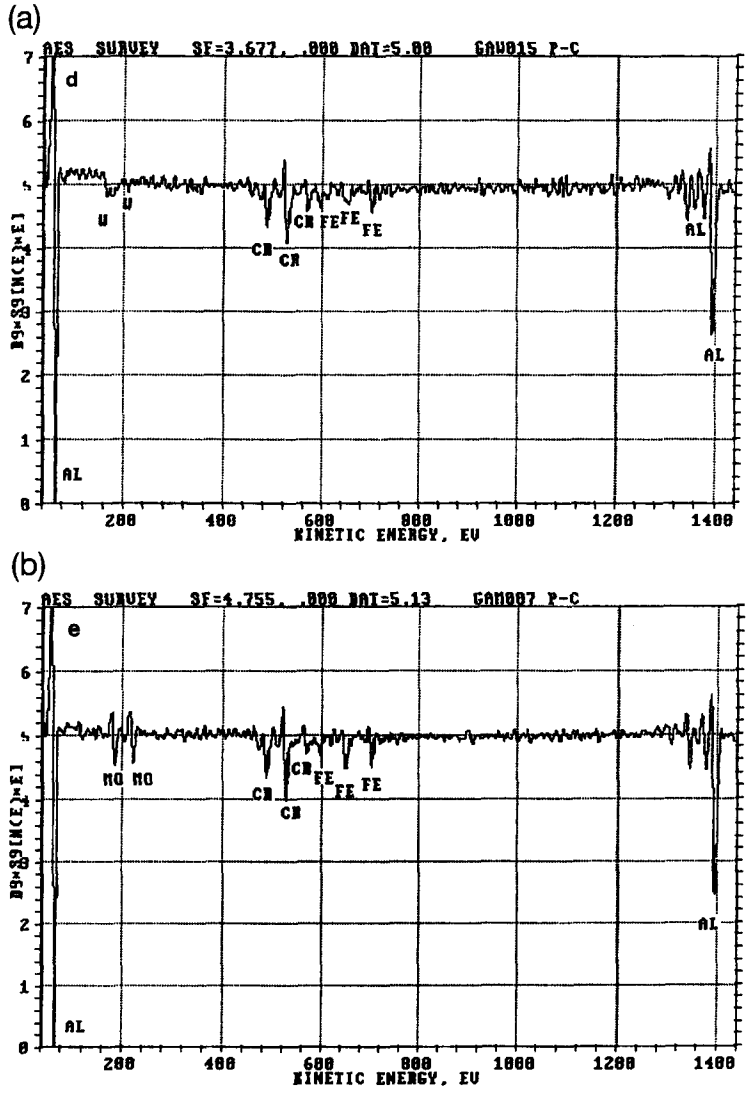

Fig. 2. AES spectra of crystals located near the aluminide layer: a) Fe–Cr–W–Al and b) Fe–Cr–Mo–Al.

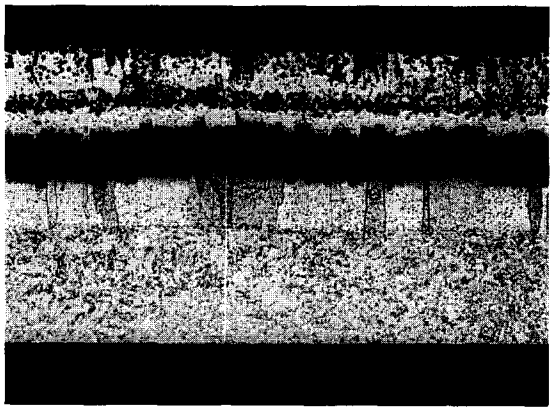

Fig. 3. Etched optical micrograph of a HDA Al–Mo specimen oxidized at 950°C for 30 h in air. The top layer and the intermediate layer are separated by a porous band.

Table 4
The result of the qualitative point analysis of the oxide scales of the Al–X specimens

	Al–W specimen (at.%)	Al–Nb specimen (at.%)	Al–Mo specimen (at.%)
Fe	0.7	0.3	0.7
Cr	0.1	0.1	0.1
O	61.0	60.4	59.3
Al	38.1	38.8	39.9

Table 5
Vickers micro hardness ($HV_{0.05}$)

Region	Al–W melt	Al–Nb melt	Al–Mo melt
Top layer	269	265	260
Intermediate layer	250	231	232

Point analyses on different areas of the scales were made for quantitative information. The average values of these measurements are listed in Table 4.

The low concentration of Fe and Cr in the scales is traced back to the favored oxidation of Al. The atomic ratio of O to Al is around 60 to 40 which corresponds to the compound Al_2O_3.

Furthermore, the element maps of Al and O were measured on the oxide scales. The oxide scale formed on the Al–W and Al–Nb specimen resp., is more uniform and dense compared to the oxide scale on the Al–Mo surface (Fig. 4).

With AES no oxide scales could be detected. An explanation could be that the hard oxide scales spalled off during polishing the cross-sections of the specimens. The two diffusion layers of the Al–X specimens were investigated with AES. The top layer consists of a single-phase compound of Al, Fe and Cr in all specimens. In the layer of the Al–W and Al–Mo specimens, some $(W, Cr)_2C$ and $(Mo, Cr)_2C$, resp., particles were identified. These particles can be found homogeneously distributed all in this layer and no enrichment could be observed. However, the carbon analysis showed no carburizing of the specimens (layer and bulk).

In the intermediate layer the gradients of Al and the steel elements are different. The Al content decreases from the band of pores to the steel side, while the steel elements show an opposite trend. The steel elements increases to the steel side. This result corresponds to previous investigations on Al specimens [6]. In this layer, none of the alloyed elements could be found. Measurements in the band of pores showed that oxygen was not present, however, only Al and the steel elements were identified.

In the top and intermediate layers, micro hardness measurements were performed. The results are listed in

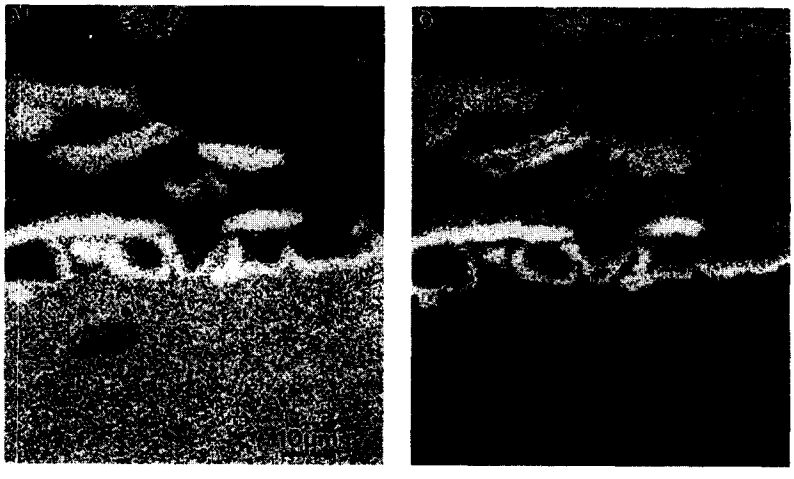

Fig. 4. XMA-element maps of aluminum and oxygen on the oxide scale of an Al–Mo specimen.

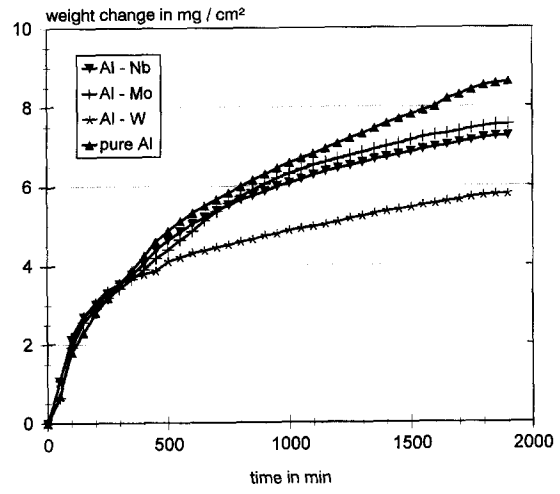

Fig. 5. Weight-gain characteristics for the oxidation of HDA specimens at 950°C up to 30 h in air.

Table 5. These values are in agreement with results presented in the literature for this composition. In the phase α-Fe(Al), Meyer et al. [16] has measured values between 600 and 110 $HV_{0.02}$. Our measurements show that the alloying elements seem to have no influence on the formed Al_xFe_y compound indicated by the unchanged values of the micro hardness.

Plots of weight gain vs. time for oxidized HDA specimens appear in Fig. 5. Consistent with these results were the observations that substantial oxide spallation had not occurred. The oxide growth curves show the similar trend for all specimens: in the beginning an initial stage of rapid oxidation followed by an interval of decreasing reaction rate. For all oxidized HDA specimens, weight gain occurred parabolically with time, which is a typical mechanism for the formation of oxide scales.

Certainly, the increase of weight change is dependent on the alloyed element. The lowest weight increase was observed by the Al–W specimens, the highest by the specimens, dipped in pure Al. The plots of Al–Mo and Al–Nb specimens lie in between the two others.

4. Discussion and conclusions

The formation of Al–X (X = W, Mo, Nb) alloys was successful just by dissolving the element X in the Al melt while stirring the system. Mo and Nb were not completely dissolved during 1 h. Only in the case of W, 1 h was enough to reach the nominal composition of the alloy. For future experiments a longer dissolving time and/or higher temperature have to be chosen. Unfortunately, our experimental arrangement is not designed for temperatures higher than 800°C.

The addition of W, Mo and Nb to the Al melt influences the HDA process and the following high temperature oxidation of the specimens as well. Although the concentration of Mo and Nb is quite low, beneficial effects can be observed.

The aluminide layer formed during the HDA process consists of the brittle intermetallic compound Al_5Fe_2, independent of the added element. Opposite to that, the thickness of the aluminide layer is changing with adding the X elements. The thinnest layers were formed on the Al–W specimens. In the Al–W and Al–Mo specimens, Fe–Cr–W–Al and Fe–Cr–Mo–Al crystals resp., could be identified in the aluminum layer near the aluminide layer. The representation of these crystals could be the reason for the decrease of the diffusion velocity of Al into the steel matrix during the HDA process.

The oxidation behavior of the Al–X specimens is dependent on the added element. In the case of the Al–W and Al–Nb specimens, the oxide scales are close and dense, unlike the Al–Mo specimens. It was observed that the internal oxidation was suppressed in the Al–X specimens while it occurred clearly in the specimens dipped in pure Al [6,7,17] and in Fe–Cr–Al alloys [18]. The reason for the suppression could be the change of the oxygen solubility of these layers [11] which results in a low oxygen potential. Already low contents of the X element are sufficient to measure the changed oxidation behavior. The largest effect was observed on the Al–W specimens where W was completely dissolved in the Al melt. The dissolution of Nb and Mo was not finished when the HDA process began. Therefore, these experiments have to be repeated with the nominal concentration for reaching a graduation for the oxidation influence of the three elements.

In the top layer of the oxidized Al–W and Al–Mo specimens $(W, Cr)_2C$ and $(Mo, Cr)_2C$ particles, resp., were observed. The source of C is not clear, however, it probably comes from the base material. During the oxidation no carburizing process has occurred which could be clearly shown by C analysis.

The following observations of the study were obtained. The adding of W, Mo and Nb to the Al melt has beneficial effects on the investigated processes.

- The thickness of the formed intermetallic layers has decreased.
- The internal oxidation during the high temperature oxidation was suppressed.
- Closer and more dense oxide scales were formed.

A range of relative effectiveness of the elements tested cannot be given because the concentrations in the Al melt were too different. The effectiveness of Nb seems to be higher than Mo but further investigation are necessary for comparison.

Acknowledgements

The authors wish to thank Mr H. Zimmermann for the metallographic and microhardness examinations and Mrs M. Green for the thermogravimetric measurements. This

work has been performed in the framework of the Nuclear Fusion Project of Forschungszentrum Karlsruhe and supported by the European Communities within the European Fusion Technology program.

References

[1] G. Benamati, A. Perujo, M. Agostini, A. Serra, N. Antolotti, Proc. 18th Symp. Fusion Technology, Karlsruhe, Germany, 1994, p. 1341.
[2] H. Glasbrenner, A. Perujo, E. Serra, Fusion Technol. 28 (1995) 1159.
[3] A. Perujo, T. Sample, E. Serra, H. Kolbe, Fusion Technol. 28 (1995) 1256.
[4] A. Terlain, E. De Vito, Proc. 18th Symp. Fusion Technology, Karlsruhe, Germany, 1994, p. 1337.
[5] A. Perujo, K.S. Forcey, T. Sample, J. Nucl. Mater. 207 (1993) 86.
[6] H. Glasbrenner, H.U. Borgstedt, J. Nucl. Mater. 212–215 (1994) 1561.
[7] H.U. Borgstedt, H. Glasbrenner, Fusion Eng. Des. 27 (1995) 659.
[8] H. Glasbrenner, Z. Peric, H.U. Borgstedt, J. Nucl. Mater. 233–237 (1996) 1378.
[9] J.K. Tien, F.S. Pettit, Metal. Trans. 3 (1972) 1587.
[10] G. Simkovich, Oxid. Met. 44 (1995) 501.
[11] Y. Shida, H. Anada, Mater. Trans. 35 (1994) 623.
[12] U.R. Kattner, in: Binary Alloy Phase Diagrams, 2nd Ed., ed. Th.B. Massalski (ASM, Metals Park, OH, 1990) p. 179.
[13] N. Saunders, in: Binary Alloy Phase Diagrams, 2nd Ed., ed. Th.B. Massalski (ASM, Metals Park, 1990) p. 174.
[14] Th. B. Massalski, ed., Binary Alloy Phase Diagrams, 2nd Ed. (ASM, Metals Park, 1990) p. 234.
[15] G. Eggeler, W. Auer, H. Kaesche, Z. Metallkd. 77 (1986) 239.
[16] L. Meyer, H.-E. Bühler, Aluminium 43 (1967) 733.
[17] H. Glasbrenner, H.U. Borgstedt, Z. Peric, in: Material Behaviour and Physical Chemistry in Liquid Metal Systems II, ed. H.U. Borgstedt (Plenum, New York, 1995) p. 95.
[18] F.H. Stott, G.C. Wood, M.G. Hobby, Oxid. Met. 3 (1971) 103.